Vibration Suppression and Defect Detection Schemes in 1D Linear Spring-Mass Systems *

Neil Jerome A. Egarguin[1,2], Taoufik Meklachi[3], Daniel Onofrei[1], and Noam D. Harari-Arnold[1]

[1]Department of Mathematics, University of Houston, Houston, TX, USA

[2]Institute of Mathematical Sciences and Physics, University of the Philippines Los Baños, Los Baños, Laguna, Philippines

[3]School of Science, Engineering, and Technology, Penn State University Harrisburg, Middletown, PA, USA

Abstract

Purpose In this paper, we present strategies for active vibration suppression and defect detection in a one-dimensional network of an arbitrary number of coupled spring–mass units connected in series. The choice of a spring–mass system is not arbitrary, as the latter is found in many applications throughout a wide range of fields, for instance in defense detection/ shielding studies, biomedical engineering, structures engineering, computer graphics and acoustics among others.

Methods The system of differential equations that model the spring–mass systems was analyzed and solved using the Laplace transform and other analytic tools. The data used in the numerical simulations were obtained by solving the associated forward problems analytically or numerically. Some of the simulations required numerical integration and minimization routines.

Results A scheme for active vibration suppression is given via explicit formulas for the required control forces. The detect defection strategy is given in terms of an explicit formula whenever only the location or mass of a lone defect is unknown and in terms of a minimization procedure whenever more than one information about the defect(s) are unknown. Several numerical simulations were done to validate these results.

Conclusion As we show in the paper, the success of the vibration suppression scheme we developed depends on the speed and accuracy of the intervening active controls. Meanwhile, the defect detection algorithm only requires measurements in a sufficiently large time interval of the longitudinal vibrations in the first mass.

1 Introduction

For many decades, spring-mass systems have been the subject of substantial research efforts due its practical relevance in almost all engineering disciplines, computer graphics and the medical field. Spring-mass systems are found in structures isolation [15, 17] , intelligent material systems, and novel devices with actuators and dampers [1, 3, 4, 19]. Furthermore, these systems are preferred

*This paper is published at the Journal of Vibration Engineering and Technologies. Complete bibliographic information is as follows: Neil Jerome A. Egarguin, Taoufik Meklachi, Daniel Onofrei, and Noam D. Harari-Arnold. Vibration Suppression and Defect Detection Schemes in 1D Linear Spring-Mass Systems. Journal of Vibration Engineering and Technologies. 2019, DOI: https://doi.org/10.1007/s42417-019-00104-5.

in computer graphics and animation to simulate the motion of cloth and hair, instead of a more physically-consistent model derived from continuum mechanics using finite elements method. In such physics-based animation modeling, high accuracy is not always necessary and spring-mass systems allow for easy implementation and fast simulation. For an in-depth discussion and survey, we refer the reader to the following articles [9, 13].

The literature involving spring-mass systems is quite extensive and a comprehensive survey is not feasible, but we will somewhat provide here a concise summary without getting into the details. For instance, in [20], cloaking in acoustic metamaterials was addressed: the authors used an infinite one-dimensional spring-mass system to experimentally realize negative and zero effective mass of the system. Another paradigm where spring-mass systems are used as models is in the study of deformable objects. In this regard, a non-rigid object is modeled as a collection of point masses linked by springs in a mesh structure [6]. In the latter paper a novel approach is introduced to achieve real-time simulation for global deformation of soft tissue using a spring-mass system. Some related work can be found in these references [7, 14, 21]. Many of these results are aimed to enhance real-time image-guided surgeries [12].

The first half of this paper deals with active vibration suppression for one dimensional spring and mass systems. In the automotive industry, active and passive vibration suppression has been successfully achieved using advanced intelligent suspension systems to improve handling and comfort [2, 16]. Since the late seventies, spring-mass networks are also used in sound synthesis to model the vibrations of musical instruments, and they are therefore classified as physical sound synthesis models [11]. However, the latter paper raised some issues regarding the accuracy of the numerical methods used. To avoid these, we will obtain exact explicit solutions of the Hookean system of ordinary differential equations (ODEs) through the inverse Laplace transform of the displacements and action forces.

In Section 3, active vibration suppression is discussed in the context of a spring-mass system of an arbitrary number of masses. The right end mass' vibration is silenced by an action force f, and a second force g intervenes to shield the vibration suppression from being communicated to mass 1 as sketched in Figure (1). We propose a control strategy that explicitly characterizes the Laplace transform of the active forces f and g needed for the desired suppression effects in a spring-mass system with unit masses and uniform spring constant and damping. In particular, we present numerical simulations of this method for two active suppression scenarios.

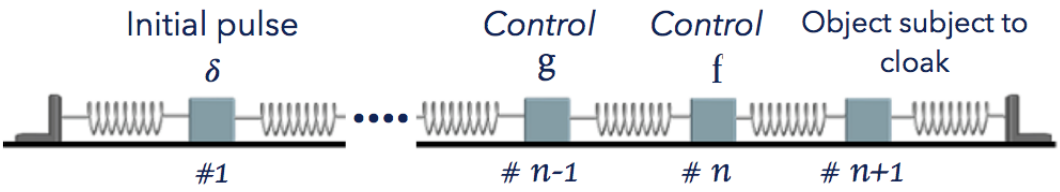

Figure 1: *A spring-mass system with n+1 unit masses*

The other half of the paper is dedicated to defect detection in a spring-mass system. As spring-mass systems appear in various physical applications, detecting and describing defects have been widely-studied. For one, defects cause some changes in the reaction of a system to external forces. For example, in [8] and [22] the effects of localized defects in periodic media, such as photonic crystal fibers in relation to light propagation were studied. Knowing some characteristics of the defects allows one to guide and control the propagation of light. Though, these studies were done in the context of continuum models in electromagnetism, the mathematical tools can be adapted for discrete systems as exhibited in [10]. A more apparent utility of defect detection is found in

industrial settings such as in automotive and other mechanical systems as well as in emerging fields of metamaterials and nanotechnology. An example of a defect detection scheme using data obtained after subjecting the system to some external excitation can be found in [18]. In said paper, surface defects on raw metal sheets in a production line were detected using infrared images obtained after subjecting the material to deflectometry. In Section 4 we propose a method of finding the location and/or mass of defects in a spring mass system configured as in Figure (2). In this set-up, n bodies are connected in series by springs with uniform stiffness constant and damping coefficient. All bodies have unit mass, except the one in position j whose mass is $m \neq 1$. At time $t = 0$ an impulse will be applied to mass 1 and the longitudinal vibrations will be measured, in the Laplace domain. These measurements will be used to find j. We also extend the method to the cases when there are more than one defect and when the masses of the defective bodies are unknown.

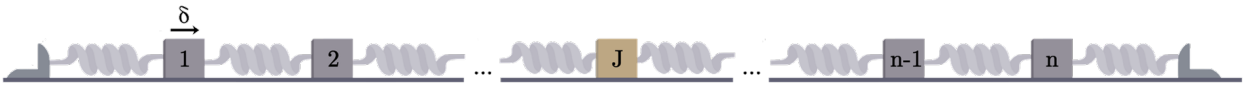

Figure 2: A spring-mass with one defect at position j.

2 Explicit solution of Spring-mass systems

In this section, we present the fundamental tools used in solving for the the longitudinal displacements and velocities in the spring-mass system when the motion is initiated by a Dirac-δ impulse on the first mass.

The model in this study consist of a coupled spring-mass system with finite number of (say n) nodes and two fixed ends, see Figure 1 or 2. Suppose that each node is of unit mass. The motion is initiated by a pulse $\gamma\delta(t)$ on node 1, where γ is a positive scaling value. When no other internal or external force is allowed to act on the system, the corresponding longitudinal displacements x_i of mass i are solutions of the following system of ODEs:

$$\begin{cases} x_1'' + dx_1' + 2kx_1 - kx_2 & = \gamma\delta(t) \\ x_2'' + dx_2' + 2kx_2 - kx_1 - kx_3 & = 0 \\ & \vdots \\ x_j'' + dx_j' + 2kx_j - kx_{j-1} - kx_{j+1} & = 0 \\ & \vdots \\ x_{n-1}'' + dx_{n-1}' + 2kx_{n-1} - kx_n - kx_{n-2} & = 0 \\ x_n'' + dx_n' + 2kx_n - kx_{n-1} & = 0 \\ x_i(0) = x_i'(0) & = 0, i = 1, 2, ..., n \end{cases} \tag{2.1}$$

where k is the stiffness constant and d is the damping force on the springs. Assuming that $k = 1$, the Laplace transform of system (2.1) is given by

$$A\tilde{x} = b \tag{2.2}$$

where

$$A = \begin{pmatrix} h & 1 & 0 & .. & .. & 0 \\ 1 & h & 1 & 0 & .. & 0 \\ .. & .. & .. & .. & .. & . \\ .. & .. & .. & .. & .. & . \\ 0 & ... & ..... & 1 & h & 1 \\ 0 & 0 & .. & .. & 1 & h \end{pmatrix}, \quad b = \begin{pmatrix} -\gamma \\ 0 \\ . \\ . \\ 0 \\ 0 \end{pmatrix}$$

and $h = -(s^2 + ds + 2)$. The following inversion theorem plays a major role in our solution to equation (2.2).

Theorem 2.1. [5] . *Let $D \leq -2$ and M be the $n \times n$ matrix*

$$M = \begin{pmatrix} D & 1 & & & & \\ 1 & D & 1 & & & \\ & 1 & D & 1 & & \\ & & \ddots & \ddots & \ddots & \\ & & & 1 & D & 1 \\ & & & & 1 & D \end{pmatrix}.$$

Then $M^{-1} = X$ is given by

$$X_{ij} = -\frac{\cosh(n + 1 - |j - i|)\lambda - \cosh(n + 1 - i - j)\lambda}{2 \sinh \lambda \sinh(n + 1)\lambda}, \tag{2.3}$$

where λ satisfies $D = -2 \cosh \lambda = -(e^{\lambda} + e^{-\lambda})$.

Since in equation (2.2), $s > 0$ then $h \leq -2$ and so Theorem 2.1 can be applied to the coefficient matrix A with $D = h = -(s^2 + ds + 2)$. Hence,

$$\tilde{x} = Rb \tag{2.4}$$

where here R denotes the inverse of A computed as in Theorem 2.1 and

$$\cosh \lambda = -\frac{h}{2} = \frac{s^2 + ds + 2}{2}. \tag{2.5}$$

The above analysis explicitly gives the analytic solution of system (2.1). To obtain the time domain solution $x(t)$ of system (2.1), one can take the inverse Laplace transform of the expressions in (2.4).

This solution framework is applicable to both of our problems, i.e., vibration suppression and defect location, with minor adjustments. Detailed discussions for each are given in the succeeding sections.

3 Active vibration suppression

In this section we consider the problem of active vibration suppression pictured in Figure 1. The goal is to design active controls f and g so that, applied on masses n and $n - 1$, respectively have the effect of suppressing the vibration of mass $n + 1$ while mass 1 does not feel any intervention, meaning mass 1 would "seem" to be affected only by the initial impulse $\gamma\delta(t)$ as the only external force in the system. In other words, in the context of an a priori known perturbation at mass 1 of the system, the two controls f, g form an active shield for any vibration coming in the system from

the right side of mass n. In this case, with forces f, g acting on masses n and $n-1$ respectively system (2.1) becomes

$$\begin{cases} x_1^{''} + 2kx_1 - kx_2 + d_1x_1^{'} & = \gamma\delta(t) \\ x_2^{''} + 2kx_2 - kx_1 - kx_3 + d_2x_2^{'} & = 0 \\ . & \\ . & \\ x_{n-1}^{''} + 2kx_{n-1} - kx_{n-2} - kx_n + d_{n-1}x_{n-1}^{'} & = g(t) \\ x_n^{''} + 2kx_n - kx_{n-1} - kx_{n+1} + d_nx_n^{'} & = f(t) \\ x_{n+1}^{''} + 2kx_{n+1} - kx_n + d_{n+1}x_{n+1}^{'} & = 0 \\ x_i(0) = x_i^{'}(0) = 0 & 1 \leq i \leq n+1 \end{cases} \tag{3.1}$$

with corresponding Laplace domain system

$$A_n\tilde{x} = b_n \tag{3.2}$$

which is an $n \times n$ system (as, by construction we set $x_{n+1} = 0$) , where

$$A_n = \begin{pmatrix} h & 1 & 0 & .. & .. & 0 \\ 1 & h & 1 & 0 & .. & 0 \\ .. & .. & .. & .. & .. & . \\ .. & .. & .. & .. & .. & . \\ 0 & ... & ..... & 1 & h & 1 \\ 0 & 0 & .. & .. & 1 & h \end{pmatrix}, \quad b_n = \begin{pmatrix} -\gamma \\ 0 \\ . \\ . \\ -\tilde{g} \\ -\tilde{f} \end{pmatrix} \quad \text{and} \quad h = -(s^2 + ds + 2).$$

The control force f is chosen such that when applied to mass n, the vibration is prevented from reaching mass $n+1$. Meanwhile the force g is designed so that when exerted on mass $n-1$, the motion of mass 1 is restored to its original state as if f had not have intervened. These controls are characterized in Theorem 3.1.

Theorem 3.1. *Consider a coupled spring-mass system connected in series, consisting of $n+1$ masses, each with mass $m = 1$ spring constant $k = 1$ and damping constant d. If the system is excited with an initial impulse $\delta(t)$ on mass 1, the Laplace transform of the control f acting on the n^{th} mass necessary to make the $(n+1)^{th}$ mass still is*

$$\tilde{f}(s) = \frac{-\sinh(3\lambda)}{\sinh(n+2)\lambda} \tag{3.3}$$

while the Laplace transform of the control g applied to the $(n-1)^{th}$ mass to restore mass 1 to its state prior to the action of control f is given by

$$\tilde{g}(s) = \frac{\sinh(2\lambda)}{\sinh(n+2)\lambda}, \tag{3.4}$$

where $\cosh(\lambda) = \frac{s^2+ds+2}{2}$.

Proof. Let $y = (y_1, y_2, ..., y_{n+1})^T$ be the displacements of the masses with only the initial impulse acting on mass 1 (without the controls f and g). Its Laplace transform, $\tilde{y} = \mathcal{L}y$, then satisfies the system of displacements:

$$A_{n+1}\tilde{y} = b_{n+1}, \tag{3.5}$$

where A_{n+1} is defined as A_n but with dimension $(n+1)\times(n+1)$, $b_{n+1} = \big(-\gamma, 0....0, 0\big)^T$ and $\gamma = 1$. The objective is to find $\tilde{f}$ and $\tilde{g}$ in system (3.2) such that $\tilde{x}_1 = \tilde{y}_1$. First, we start by solving for $\tilde{y}_1$ in (3.5). Let $R' = A_{n+1}^{-1}$, then we have

$$\tilde{y} = R' b_{n+1}$$

which implies

$$\tilde{y}_1 = -R'_{1,1}.$$

Using (2.3) gives

$$\tilde{y}_1 = \frac{\sinh(n+1)\lambda}{\sinh(n+2)\lambda} = \tilde{x}_1. \tag{3.6}$$

Now that $\tilde{x}_1$ is evaluated and $\tilde{x}_n$ is set to 0, which is an immediate consequence of the condition $\tilde{x}_{n+1} = 0$, we proceed by writing the first and n^{th} rows of the system $\tilde{x} = Rb_n$ as follows:

$$\begin{aligned}\tilde{x}_1 &= -R_{1,1} - \tilde{g}R_{1,n-1} - \tilde{f}R_{1,n}\\ \tilde{x}_n &= -R_{n,1} - \tilde{g}R_{n,n-1} - \tilde{f}R_{n,n}.\end{aligned}$$

The solution of the above linear system of $\tilde{f}$ and $\tilde{g}$ are given by:

$$\tilde{f} = \frac{R_{n,n-1}\tilde{x}_1 - R_{n,1}R_{1,n-1} + R_{n,n-1}R_{1,1}}{R_{n,n}R_{1,n-1} - R_{n,1}R_{n,n-1}}$$

$$\tilde{g} = \frac{{R_{1,n}}^2 - {R_{1,1}}^2 - R_{n,n}\tilde{x}_1}{R_{n,n}R_{1,n-1} - R_{n,1}R_{n,n-1}}.$$

Plugging-in the R_{ij} coefficients from (2.3), the interventions $\tilde{f}$ and $\tilde{g}$ take the forms

$$\begin{aligned}\tilde{f}(s) &= \frac{-\sinh(3\lambda)}{\sinh(n+2)\lambda}\\ \tilde{g}(s) &= \frac{\sinh(2\lambda)}{\sinh(n+2)\lambda}\end{aligned}$$

where λ is defined by the relation $\cosh(\lambda) = -\frac{h}{2} = \frac{s^2+ds+2}{2}$. □

To verify that the uniquely computed controls perfectly quiet mass $n+1$ while keeping mass 1 unaware of what happened, we substitute $\tilde{f}$ and $\tilde{g}$ in the Laplace transform of the system (3.1) given by

$$A_{n+1}\tilde{x} = b'_{n+1},$$

where A_{n+1} is as defined in (3.5) and $b'_{n+1} = \big(-\gamma, 0....\tilde{f}, \tilde{g}, 0\big)^T$. We then have $\tilde{x} = R'b'_{n+1}$. Straightforward algebra shows that $\tilde{x}_{n+1} = 0$ (the vibration suppression of mass n+1 is successfully performed) and $\tilde{x}_1 = \tilde{y}_1$ (shielding of the vibration suppression from being communicated to mass 1 is also verified).

In what follows we will offer some numerical simulations to support the results discussed above and to show how exactly controls analytically predicted by formulas (3.3) and (3.4) work in covertly silencing any vibration present in mass $n+1$ thus rendering their own action as well as vibrations at mass $n+1$ invisible through measurements at the location of the initial input, i.e., mass 1.

For the subsequent numerics we further assume a $\gamma\delta(t)$ impulse on mass 1 ("interrogator" location), with $\gamma = 1$. Mass n is the location where the control f is acting to prevent the propagating

pulse from interacting with the end mass $n+1$ (the target subject to cloak). The control force f, acting alone, would cause the system to behave differently, hence mass 1 would feel the response. Fortunately, a new control g on mass $n-1$ will successfully restore the displacement profile of mass 1 as if no interventions took place. In what follows for the numerical support of our general results, we will consider a coupled spring-mass system with $n=5$ and respectively $n=20$ nodes and two fixed ends. The controls f and g are computed in the two systems of 5 and 20 masses to illustrate different scenarios and we assumed that the spring constant $k=1$ and the damping coefficient $d=0.1$ in all the springs.

3.1.1 *System of* 5 *springs.* We have from (3.3) and (3.4), for $n=4$:

$$\tilde{f}(s) = \frac{-\sinh 3\lambda}{\sinh 6\lambda} \tag{3.7}$$

$$\tilde{g}(s) = \frac{\sinh 2\lambda}{\sinh 6\lambda}. \tag{3.8}$$

By performing the substitution

$$\lambda = \cosh^{-1}\left(\frac{s^2+ds+2}{2}\right),$$

we are able to invert the Laplace transforms and obtain explicit formulas for the controls f and g. The plots of these controls are shown in Figure 3. The next plots illustrate that

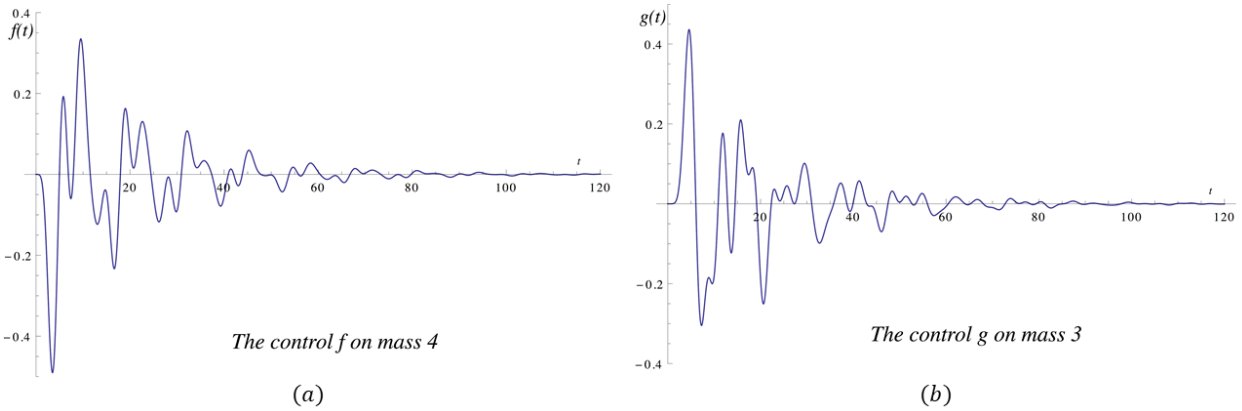

Figure 3: (a) Plots of controls f and g.

indeed cloaking is achieved, i.e., the two control forces f and g are making the last mass motionless while their intervention is completely 'invisible' to an observer measuring the vibrations echos felt by the first mass. Indeed, Figure 4 compares the vibrations x_1 before and after the application of the suppression control f alone. It is evident that the action of f alone, while rendering the last mass motionless, altered the vibrations of x_1 when compared to the case of no controls thus making the action visible to an observer at mass 1. On the other hand, after the application of the second control g, besides rendering the last mass motionless we also observe that the vibrations of the first mass are restored to the state prior to the action of the two controls, thus making the action of the two controls invisible to an observer measuring the vibrations of the first mass. See Figure 5.

3.1.2 *System of* 20 *masses.* In this subsection we study the case of 20 masses, which is also a test for the algorithm's effectiveness against the numerical challenges that comes with a high number

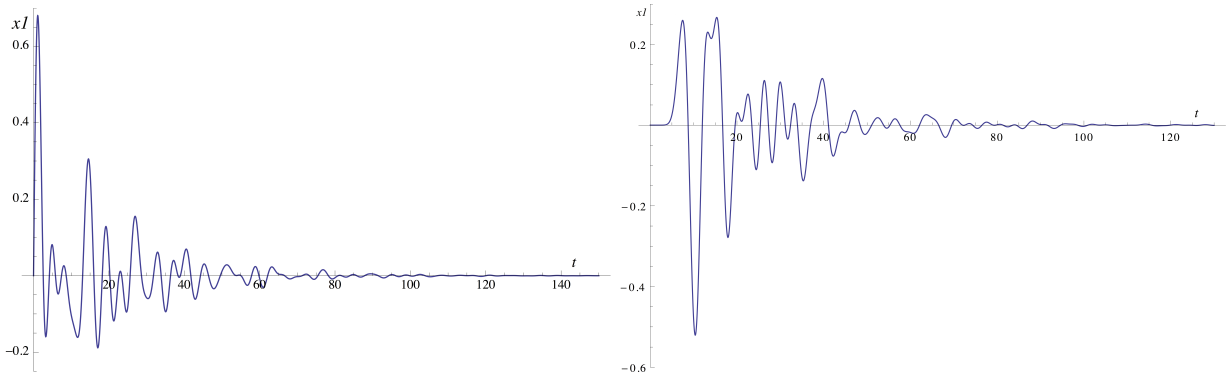

(a) x_1 without the controls f and g

(b) x_1 with suppression control f but without the cloaking control g

Figure 4: Plots illustrating the effects of the suppression control f.

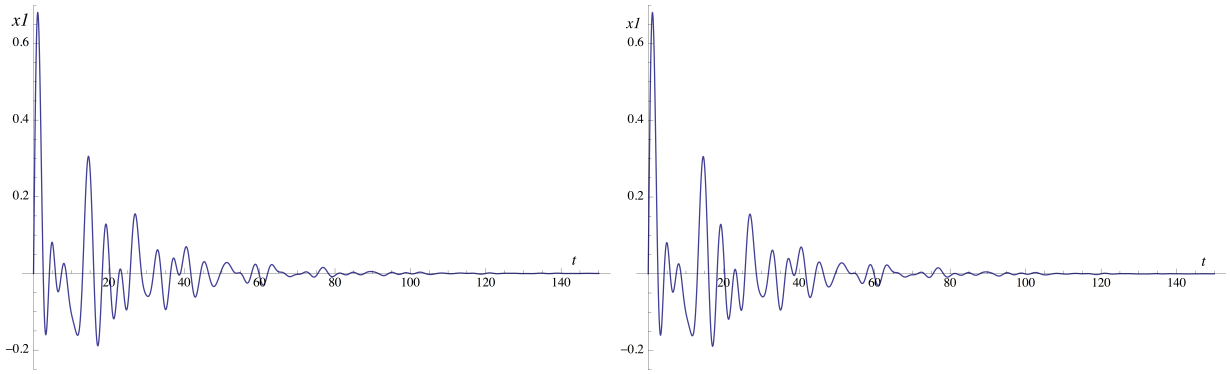

(a) x_1 without the controls f and g

(b) x_1 with both controls f and g

Figure 5: Plots illustrating the effects on x_1 of the controls f and g acting together while last mass is motionless.

of masses as posed in [11]. In this case, we numerically compute the inverse Laplace transform of $\tilde{f}$ and $\tilde{g}$. Thus, similar to the 5-mass case presented before, the Laplace transform of f and g are given by the expressions:

$$\tilde{f}(s) = \frac{-\sinh 3\lambda}{\sinh 21\lambda}$$
$$\tilde{g}(s) = \frac{\sinh 2\lambda}{\sinh 21\lambda}.$$

The inverse Laplace transform of $\tilde{f}$ and $\tilde{g}$, computed numerically are shown in Figure 6. Due to the presence of more masses in the model the expected time delay can be visually observed for the two active controls since they begin their action immediately after the pulse applied at mass 1 propagates to the last mass. Now, we illustrate the effects of these controls to the system. Figure 7 compares the vibrations in x_1 prior to the application of any control and after the action of the suppression control f.

In Figure 8 it can be observed that indeed after the application of the second control g, the

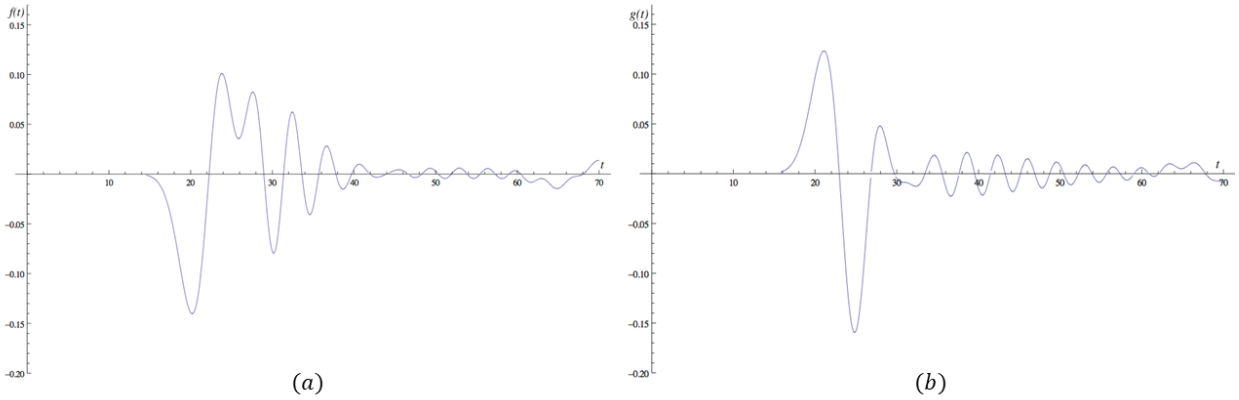

(a) (b)

Figure 6: (a) f exerted on mass 19. (b)g exerted on mass 18.

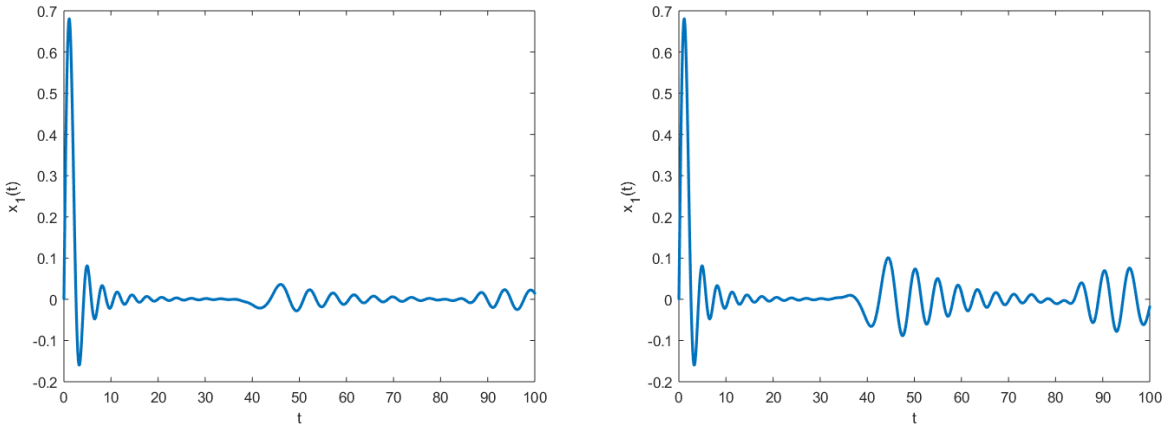

(a) x_1 without the controls f and g

(b) x_1 with suppression control f but without the cloaking control g

Figure 7: Plots illustrating the effects of the suppression control f.

vibrations on x_1 were restored to its state prior to the action of both controls.

Another consequence of Theorem 2.1 is the possibility of simulating a vibration suppression scheme in a one dimensional spring mass system by using only one control. Unlike in the previous section, we will perform a complete isolation of mass n without trying to restore the displacement of mass 1 with the help of an extra control g. This question could be relevant to the problem of designing a good vibration suppression scheme in a car suspension system.

For this application, we only suppress the vibration from reaching mass $n+1$ by a forcing control f actively and instantaneously engaged on mass n, see Figure 9. Our purpose here is to attain a robust annihilation of the vibrations felt at mass $n+1$ of the system by implementing an efficient evaluation process to compute the necessary control force f.

The main result for this application is stated in the Corollary 3.2 that gives the Laplace transform of the required control f for the vibration suppression of the last mass in a spring-mass system of $n+1$ number of masses.

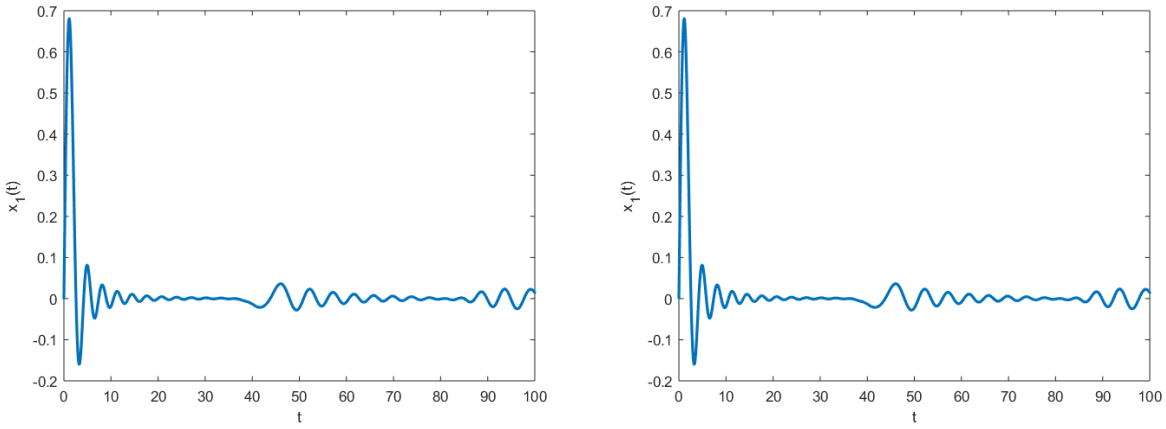

(a) x_1 without the controls f and g (b) x_1 with both controls f and g

Figure 8: Plots illustrating the effects on x_1 of the controls f and g acting together while last mass is motionless.

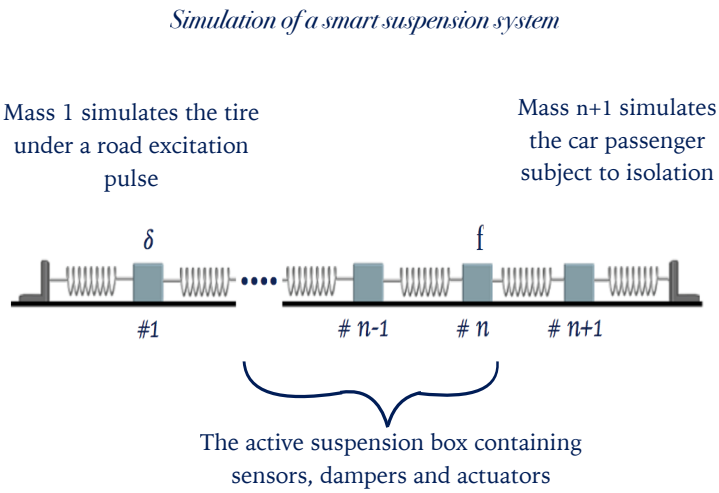

Figure 9: Illustration of the model of a smart suspension system in a car

Corollary 3.2. *Consider a coupled spring-mass system connected in series, consisting of* $(n+1)$ *masses, each with mass* $m = 1$ *with uniform spring constant* $k = 1$ *and under a damping constant* d*. If the system is excited with an initial impulse* $\delta(t)$ *on mass 1, the Laplace transform of the control* f *acting on the* n^{th} *mass necessary to make the* $(n+1)^{th}$ *still is:*

$$\tilde{f}(s) = -\frac{\sinh(\lambda)}{\sinh(n\lambda)} \tag{3.9}$$

where

$$\cosh(\lambda) = \frac{s^2 + ds + 2}{2}.$$

Proof. We will proceed by using the Theorem 2.1 to analytically compute the inverse of the tridiagonal matrix A_n to solve for $\tilde{x}_n$ in terms of $\tilde{f}$ in the system $A_n\tilde{x} = b_n$ as defined in (3). The

condition on mass $n+1$ to be still implies that mass n to be still as well, hence $\tilde{x}_n = 0$.

$$A_n = \begin{pmatrix} h & 1 & 0 & .. & .. & 0 \\ 1 & h & 1 & 0 & .. & 0 \\ .. & .. & .. & .. & .. & . \\ .. & .. & .. & .. & .. & . \\ 0 & ... & ..... & 1 & h & 1 \\ 0 & 0 & .. & .. & 1 & h \end{pmatrix}, \quad b_n = \begin{pmatrix} -1 \\ 0 \\ . \\ . \\ 0 \\ -\tilde{f} \end{pmatrix} \quad and \quad h = -(s^2 + ds + 2) \tag{3.10}$$

In fact,

$$\tilde{x}_n = -R_{n1} - \tilde{f} R_{nn} = 0,$$

which implies:

$$\tilde{f} = -\frac{R_{n1}}{R_{nn}}.$$

Formula (2.3) enables us to evaluate both R_{n1} and R_{nn} and obtain $\tilde{f}$ in a simplified form:

$$\tilde{f} = -\frac{\sinh(\lambda)}{\sinh(n\lambda)}.$$

□

4 Defect Detection

In this section, we develop an algorithm to find the location of a defect in a spring-mass system. We consider a system of n nodes each of which has unit mass, except for some defective nodes, i.e., the defects, which may have different mass. We start with a detailed solution of the case of a single defect with unknown location but a priori known mass $m = m_1$, then extend the results to cases such as a single defect of unknown mass and location, and multiple defects with known or unknown masses. In all the systems used in the numerical simulations, the spring constant is $k = 1$ and the damping coefficient is $d = 0.1$.

4.1 One defect of unknown location

Consider a system of n masses with exactly one defect, say in position j with mass m. Adjacent masses in this system are connected by springs of the same stiffness constant k and damping coefficient d. We apply an impulse of magnitude γ on the first mass to initiate vibrations in the system. The goal is to determine j and possibly m using some measurements of the displacement of the first mass x_1 over a time interval. With these assumptions, we derive the following modification

of system (2.1):

$$\begin{cases} x_1'' + dx_1' + 2kx_1 - kx_2 & = \gamma\delta(t) \\ x_2'' + dx_2' + 2kx_2 - kx_1 - kx_3 & = 0 \\ & \vdots \\ m\ x_j'' + dx_j' + 2kx_j - kx_{j-1} - kx_{j+1} & = 0 \\ & \vdots \\ x_{n-1}'' + dx_{n-1}' + kx_{n-1} - kx_n - kx_{n-2} & = 0 \\ x_n'' + dx_n' + 2kx_n - kx_{n-1} & = 0 \\ x_i(0) = x_i'(0) & = 0, i = 1, 2, ..., n \end{cases} . \tag{4.1}$$

Taking $k = 1$, the corresponding system in the Laplacian domain is the following vector equation:

$$\hat{A}\tilde{x} = \begin{pmatrix} -\gamma \\ 0 \\ \vdots \\ 0 \end{pmatrix} \tag{4.2}$$

where

$$\hat{A} = \begin{pmatrix} h & 1 & & & & & & & \\ 1 & h & 1 & & & & & & \\ & 1 & h & 1 & & & & & \\ & & \ddots & \ddots & \ddots & & & & \\ & & & 1 & -\left(ms^2 + ds + 2\right) & 1 & & & \\ & & & & \ddots & \ddots & \ddots & & \\ & & & & & 1 & h & 1 & \\ & & & & & & 1 & h & \end{pmatrix}$$

with $h = -(s^2 + ds + 2)$ and the quantity $-(ms^2 + ds + 2)$ is in the j^{th} row.

Let $M = \begin{pmatrix} h & 1 & & & & \\ 1 & h & 1 & & & \\ & 1 & h & 1 & & \\ & & \ddots & \ddots & \ddots & \\ & & & 1 & h & 1 \\ & & & & 1 & h \end{pmatrix}$ as in Theorem 2.1 with $D = h$. Consider $E = \hat{A} - M$ and observe that E is the matrix with the only nonzero entry given by $E_{jj} = (1 - m)s^2$. With $b = (-\gamma, 0, 0, ..., 0)^T$ and by Theorem 2.1, equation (4.2) can be solved as follows:

$$\begin{aligned} (M + E)\tilde{x} &= b \\ \tilde{x} + RE\tilde{x} &= Rb, \end{aligned} \tag{4.3}$$

where $R = M^{-1}$. It then follows that for $i = 1, ..., n$:

$$\begin{aligned} \tilde{x}_i + R_{ij}(1 - m)s^2\tilde{x}_j &= -\gamma R_{i1} \\ \tilde{x}_i &= -\gamma R_{i1} - R_{ij}(1 - m)s^2\tilde{x}_j \end{aligned} \tag{4.4}$$

In particular, if $i = j$, we have

$$\tilde{x}_j(s) = \frac{-\gamma R_{j1}}{1 + R_{jj}(1-m)s^2}. \tag{4.5}$$

Also, putting in $i = 1$ in (4.4) and using (4.5) and the fact that $R_{1j} = R_{j1}$ we get the following expression for $\tilde{x}_1$:

$$\tilde{x}_1(s) = -\gamma R_{11} - R_{1j}(1-m)s^2 \cdot \frac{-\gamma R_{j1}}{1 + R_{jj}(1-m)s^2}. \tag{4.6}$$

From hereon, we consider the particular case when $\gamma = 1$ and so (4.6) becomes

$$\tilde{x}_1(s) = -R_{11} + R_{1j}(1-m)s^2 \cdot \frac{R_{j1}}{1 + R_{jj}(1-m)s^2}. \tag{4.7}$$

By computing the Laplace transform of experimental time domain data x_1 obtained by actual measurements of the vibrations in the spring mass system, one can solve for j in equation (4.7). However, this equation can be simplified by looking at the asymptotic behavior of R_{jj} as s becomes large. From (2.5), we have for sufficiently large s:

$$\lambda = \cosh^{-1}\left(\frac{s^2 + ds + 2}{2}\right) \approx \cosh^{-1}\left(\frac{s^2}{2}\right) = \ln\left(\frac{s^2}{2} + \sqrt{\frac{s^4}{4} - 1}\right) \approx \ln s^2. \tag{4.8}$$

Using (4.8) in the expansion for R_{jj} given in (2.3) yields

$$\begin{aligned} R_{jj} &= -\frac{\cosh((n+1)\lambda) - \cosh((n+1-2j)\lambda)}{2\sinh(\lambda)\sinh((n+1)\lambda)} \\ &\approx -\frac{s^{2(n+1)} + s^{-2(n+1)} - s^{2(n+1-2j)} - s^{-2(n+1-2j)}}{(s^2 - s^{-2})(s^{2(n+1)} - s^{-2(n+1)})} \\ &\approx -\frac{s^{2(n+1)} - s^{2(n+1-2j)}}{s^2 s^{2(n+1)}} = -\frac{1 - s^{-4j}}{s^2} \\ &\approx -\frac{1}{s^2}. \end{aligned} \tag{4.9}$$

Using this last result in (4.7) gives

$$\begin{aligned} \tilde{x}_1(s) &= -R_{11} + \frac{R_{1j}^2(1-m)s^2}{R_{jj}(1-m)s^2}\left(\frac{1}{\frac{1}{R_{jj}(1-m)s^2} + 1}\right) \\ &\approx -R_{11} + \frac{R_{1j}^2}{R_{jj}}\left(\frac{1}{\frac{1}{m-1} + 1}\right) \\ &= -R_{11} + \frac{m-1}{m} \cdot \frac{R_{1j}^2}{R_{jj}}. \end{aligned} \tag{4.10}$$

This last estimate for $\tilde{x}_1(s)$ can be used to find j for a sufficiently large value of s. Using (2.3), (4.10) can be written as

$$\cosh(j\lambda) \approx \frac{-2m\tilde{x}_1(s)\sinh((n+1)\lambda) + (m+1)\sinh(n\lambda) + |m-1|\sinh((n+2)\lambda)}{\sqrt{2m\left[C_1\cosh(2(n+1)\lambda) - C_2\cosh((2n+3)\lambda) - C_3\cosh((n+1)\lambda) + C_4\cosh\lambda + \cosh(2n\lambda) + C_5\right]}} \tag{4.11}$$

where the coefficients in the denominator are given by

$$\begin{aligned} C_1 &= m(\tilde{x}_1(s))^2 + m - 1 \\ C_2 &= (m-1)\tilde{x}_1(s) \\ C_3 &= (m+1)\tilde{x}_1(s) \\ C_4 &= 2m\tilde{x}_1(s) \\ C_5 &= m^2[-(\tilde{x}_1(s))^2 - 2 + m]. \end{aligned} \tag{4.12}$$

Using the asymptotics in (4.8), the hyperbolic functions in (4.11) can be expressed as sums of powers of s:

$$\cosh(p\lambda) \approx \frac{s^{2p} + s^{-2p}}{2} \text{ and } \sinh(p\lambda) \approx \frac{s^{2p} - s^{-2p}}{2}, p \in \mathbb{R}. \tag{4.13}$$

Then using (4.13) and the fact that $\tilde{x}_1(s)$ decays for large s, it can be shown that as s increases the numerator of (4.11) tends to $+\infty$ while the denominator decays to 0 via positive values. Hence, the right hand side of (4.11) is greater than 1 for large enough s, allowing us to write the following formula for j:

$$j \approx \frac{\cosh^{-1}\left(\dfrac{-2m\tilde{x}_1(s)\sinh((n+1)\lambda) + (m+1)\sinh(n\lambda) + |m-1|\sinh((n+2)\lambda)}{\sqrt{2m\left[C_1\cosh(2(n+1)\lambda) - C_2\cosh((2n+3)\lambda) - C_3\cosh((n+1)\lambda) + C_4\cosh\lambda + \cosh(2n\lambda) + C_5\right]}}\right)}{\lambda}. \tag{4.14}$$

4.1.1 We illustrate the process described above. Consider a system of 20 masses with exactly one defect at $j = 15$ of mass $m = 1.01$. Numerically, the time domain solution of the corresponding system (4.1) in this context can be obtained and Figure 10 shows the displacement x_1 of the first mass as a function of time. Then the Laplace transform of this time domain solution is calculated and used as the "simulated data" (to be replaced in reality by time actual measurements of displacement x_1) in (4.14) to obtain an approximation for j. Figure 11 shows that, as expected, the computed values of j approaches 15 as s becomes large. In fact, at $s = 50$, the computed value of j is around 15.0898, incurring a small relative error of around 0.60%

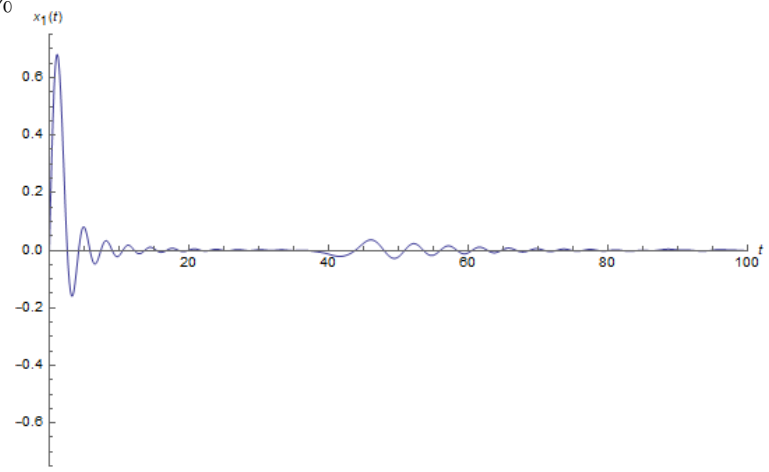

Figure 10: The displacement x_1 of the first mass in the system with $n = 20, j = 15$ and $m = 1.01$.

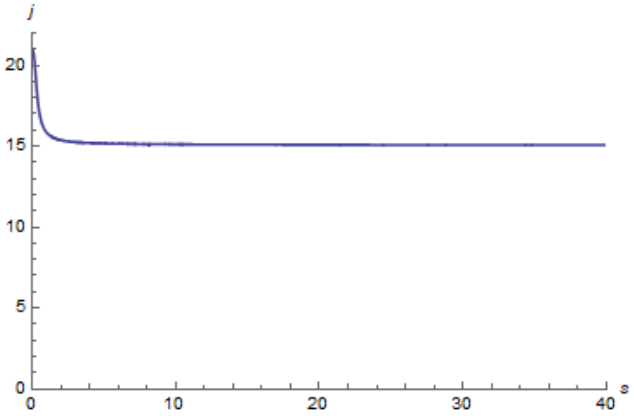

Figure 11: The approximations for the value of j for a given s in the system with $n = 20, j = 15$ and $m = 1.01$. Notice that the approximations approaches the location $j = 15$ of the defect as s increases.

Figure 10 indicates that, in reality, the time duration for the actual measurements of x_1 is finite and may be small depending on the value of the damping coefficient d. Also, note that although (4.14) gives an explicit way of approximating the location of the defect in a system, it requires a knowledge of the value of m. Moreover, the formula is quite complex as many function evaluations are performed. This formula can be simplified for the case when the defect is large, that is, when $m \gg 1$. With this new assumption and for large s, (4.7) can be written as

$$\tilde{x}_1(s) \approx -R_{11} + \frac{R_{j1}^2}{R_{jj}}. \tag{4.15}$$

Again, using (2.3) the relation (4.15) can be rewritten as

$$\cosh j\lambda \approx \frac{\cosh\lambda - x_1(s)}{\sqrt{(\tilde{x}_1(s))^2 - 2\tilde{x}_1(s)\cosh\lambda + 1}}. \tag{4.16}$$

Clearly, the numerator of (4.16) increases without bounds as s increases. Meanwhile, with the use of (2.5) and the Initial Value Theorem for Laplace transforms, one can show that the denominator is approximately equal to 1 for large s. Thus, the right hand side of (4.16) is greater than 1 for sufficiently large s and so

$$j \approx \frac{\cosh^{-1}\left(\dfrac{\cosh\lambda - x_1(s)}{\sqrt{(\tilde{x}_1(s))^2 - 2\tilde{x}_1(s)\cosh\lambda + 1}}\right)}{\lambda} \tag{4.17}$$

is a well-defined approximation. Now, this formula for j involves less calculations and prior knowledge of the exact value of m is not necessary. All that is required for (4.17) to work is that the mass of the defect is far from the uniform mass 1. We illustrate this new procedure for a five- and a 20-mass system.

4.1.2 Consider the system of five masses with defect at $j = 3$ and $m = 4$. Numerically the time domain solution of the corresponding system (4.1) can be obtained. Figure 12 shows the plot of the displacement of the first mass. Again, the Laplace transform $\tilde{x}_1$ of this solution is computed and used as "simulated data " input in (4.17). Figure 13 shows the plot of the

approximates obtained as a function of s. Again, fast convergence to $j = 3$ can be observed. In fact, when $s = 50$, the computed value of j is approximately 3.018423, with relative error of around 0.61%.

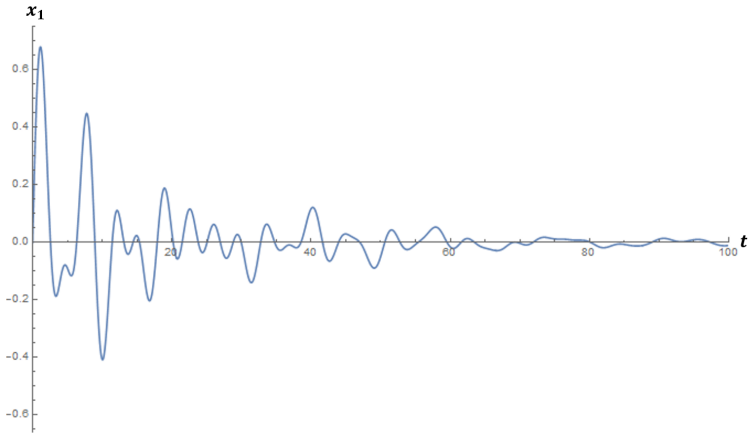

Figure 12: Plot of the movement x_1 of the first mass in the system with $n = 5, j = 3$, and $m = 4$.

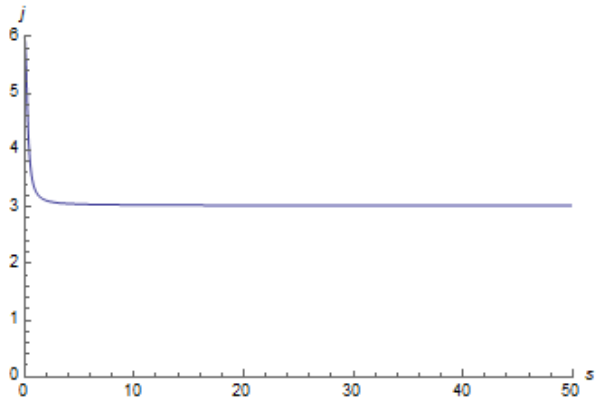

Figure 13: Plot of the approximations for the value of j for a given s.

4.1.3 We now try the formula for a larger system. Consider 20 masses with defect at $j = 3$ and $m = 5$. Similar calculations as above will produce the results shown in Figures 14 and 15. It is worth noting from Figure 15 that the convergence of $j(s)$ to the actual position of the defect is still very fast. Here at $s = 50$, the computed approximate for j is 3.01429, with relative error of just below 0.48%.

4.2 Multiple defects with unknown location and/or mass

Now we develop a scheme for the case when there are more than one unknown information about the defect/s in the system. Here we deal with systems with at most two defects though the solution schemes can be extended to cases with more defects. Let $\tilde{x}_1^*$ be the Laplace transform of the time domain solution for the displacement of the first mass in the system. This function will be used again as the input "simulated data" for our numerical procedure. The solution described below

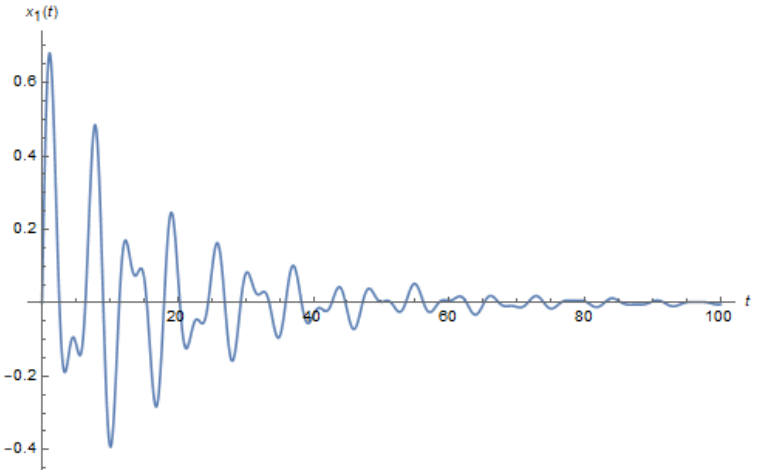

Figure 14: Plot of the movement x_1 of the first mass in the system with $n = 20, j = 3$, and $m = 5$.

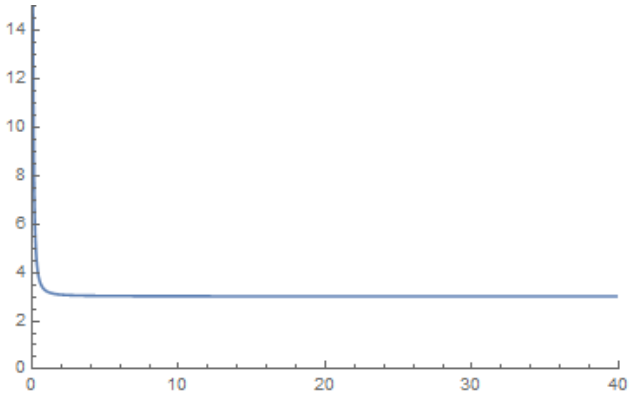

Figure 15: Plot of the approximations for the value of j for a given s.

involves the minimization of the L^2 residual function

$$r(\cdot) = \int_0^{+\infty} |\tilde{x}_1(s, \cdot) - \tilde{x}_1^*(s)|^2 \, ds, \tag{4.18}$$

where $\tilde{x}_1$ is the approximation to $\tilde{x}_1^*$ obtained by solving the corresponding system of ODEs using the Inversion Theorem 2.1, treated as a function of s and the unknown problem parameters. In the following examples, this procedure is implemented for the different cases of multiple unknown defect parameters. In all numerical simulations below, the integration in (4.18) is performed numerically via Matlab's intrinsic integral function. In doing so, the integral's upper bound is replaced by 300, since both terms in the integrand decays fast to zero.

4.2.1 *One defect with unknown location and mass.* We begin with the case when there is exactly one defect of unknown location and mass. In (4.7), we saw that using the Inversion Theorem 2.1 in solving the Laplace domain system (4.2) yields

$$\tilde{x}_1(s, j, m) = -R_{11} + R_{1j}(1 - m)s^2 \cdot \frac{R_{j1}}{1 + R_{jj}(1 - m)s^2}, \tag{4.19}$$

which can treated as a function of the unknowns j and m. Since there are only two unknowns, a visual inspection of the 3D plot of the residual function r can be done to find its minimizers.

To illustrate this, we consider a system of $n = 20$ masses, with exactly one defect at location 10 of mass 3. In lieu of actual measurements, the input data $\tilde{x}_1^*$ is numerically obtained by first solving (4.1) explicitly and then computing the solution's Laplace transform. The 3D plot of the residual function

$$r(j,m) = \int_0^{+\infty} |\tilde{x}_1(s,j,m) - \tilde{x}_1^*(s)|^2 \, ds$$

for various values of j and m are shown in Figure 16(a). From this graph we obtain the location and mass of the defect by observing the minimizer of r. Figures 16(b) and (c) show 2D projections of the graph of r suggesting that indeed the minimum occurs at the point with $j = 10$ and $m = 3$.

4.2.2 *Two defects with unknown locations but known masses.* Now suppose that the system has exactly two defects at locations j_1 and j_2 with known masses m_1 and m_2, respectively. These new assumptions will introduce minor modifications to system (4.1) giving rise to the following Laplace domain system:

$$\hat{A}\tilde{x} = \begin{pmatrix} -1 \\ 0 \\ \vdots \\ 0 \end{pmatrix} \tag{4.20}$$

where

$$\hat{A} = \begin{pmatrix} h & 1 & & & & & & & & \\ 1 & h & 1 & & & & & & & \\ & \ddots & \ddots & \ddots & & & & & & \\ & & 1 & -\left(m_1 s^2 + ds + 2\right) & 1 & & & & & \\ & & & \ddots & \ddots & \ddots & & & & \\ & & & & 1 & -\left(m_2 s^2 + ds + 2\right) & 1 & & & \\ & & & & & \ddots & \ddots & \ddots & & \\ & & & & & & 1 & h & 1 & \\ & & & & & & & 1 & h \end{pmatrix}$$

with $h = -(s^2 + ds + 2)$ and the quantities $-(m_1 s^2 + ds + 2)$ and $-(m_2 s^2 + ds + 2)$ are in the j_1^{th} and j_2^{th} row, respectively. This system can be solved using similar techniques as in (4.3)-(4.7), except that this time the matrix E will have two nonzero entries $E_{j_1 j_1} = (1 - m_1)s^2$ and $E_{j_2 j_2} = (1 - m_2)s^2$. Performing the calculations will give for $i = 1, 2, ..., n$:

$$\tilde{x}_i(s) + R_{ij_1}(1 - m_1)s^2 \tilde{x}_{j_1}(s) + R_{ij_2}(1 - m_2)s^2 \tilde{x}_{j_2}(s) = -R_{1i}. \tag{4.21}$$

In particular, using $1, j_1$ and j_2 as the value of i in (4.21) gives the system:

$$\begin{cases} \tilde{x}_1(s) &= -R_{11} - R_{1j_1}(1 - m_1)s^2 \tilde{x}_{j_1}(s) - R_{1j_2}(1 - m_2)s^2 \tilde{x}_{j_2}(s) \\ \tilde{x}_{j_1}(s) &= \dfrac{-R_{1j_1} - R_{j_1 j_2}(1 - m_2)s^2 \tilde{x}_{j_2}(s)}{1 + R_{j_1 j_1}(1 - m_1)s^2} \\ \tilde{x}_{j_2}(s) &= \dfrac{-R_{1j_2} - R_{j_1 j_2}(1 - m_1)s^2 \tilde{x}_{j_1}(s)}{1 + R_{j_2 j_2}(1 - m_2)s^2} \end{cases} . \tag{4.22}$$

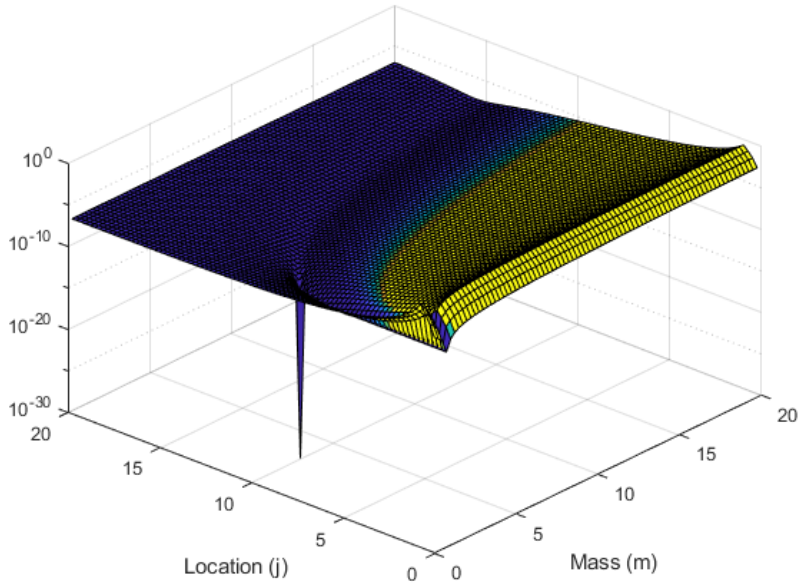

(a) 3D plot of r

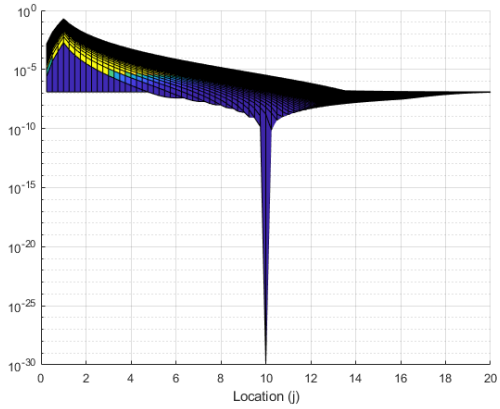

(b) 2D projection of the graph of r showing the j-axis

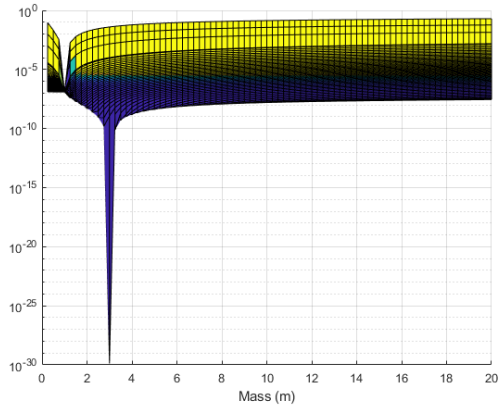

(c) 2D projection of r showing the m-axis.

Figure 16: Different views of the the graph of plot of the L^2 residual function r.

Solving for $\tilde{x}_1(s)$ in (4.22) yields

$$\tilde{x}_1(s) = \frac{-R_{11} + s^2\Big((1-m_1)R_{1j_1}^2 - (m_2-1)R_{1j_2}^2 + (m_1-1)R_{11}R_{j_1j_1} + (m_2-1)R_{11}R_{j_2j_2}\Big) + s^4(m_1-1)(m_2-1)(R_{1j_2}^2R_{j_1j_1} - 2R_{1j_1}R_{1j_2}R_{j_1j_2} + R_{11}R_{j_1j_2}^2 + R_{1j_1}^2R_{j_2j_2} - R_{11}R_{j_1j_1}R_{j_2j_2})}{1 + s^2\Big((1-m_1)R_{j_1j_1} + (1-m_2)R_{j_2j_2} + s^2(m_1-1)(m_2-1)\big(R_{j_1j_1}R_{j_2j_2} - R_{j_1j_2}^2\big)\Big)} \tag{4.23}$$

Since the locations of the defects are unknown, we shall treat $\tilde{x}_1$ as function of s, j_1 andj_2, and compare it with experimental data $\tilde{x}_1^*$.

In the example below, we consider a system of 20 masses with exactly two defects at unknown locations $j_1 = 10$ and $j_2 = 15$. We assume that the masses $m_1 = 3$ and $m_2 = 7$ of the defects

are known. As before we define the L^2-residual function r as

$$r(j_1, j_2) = \int_0^{+\infty} |\tilde{x}_1(s, j_1, j_2) - \tilde{x}_1^*(s)|^2 \, ds.$$

Different views of the 3D plot of r are shown in Figure 17. The 3D rendering of the graph in Figure 17-(a) suggests that r has s a unique minimum. The two-dimensional projections of this graph indicate that this minimum occurs somewhere near the point with $j_1 = 10$ and $j_2 = 15$.

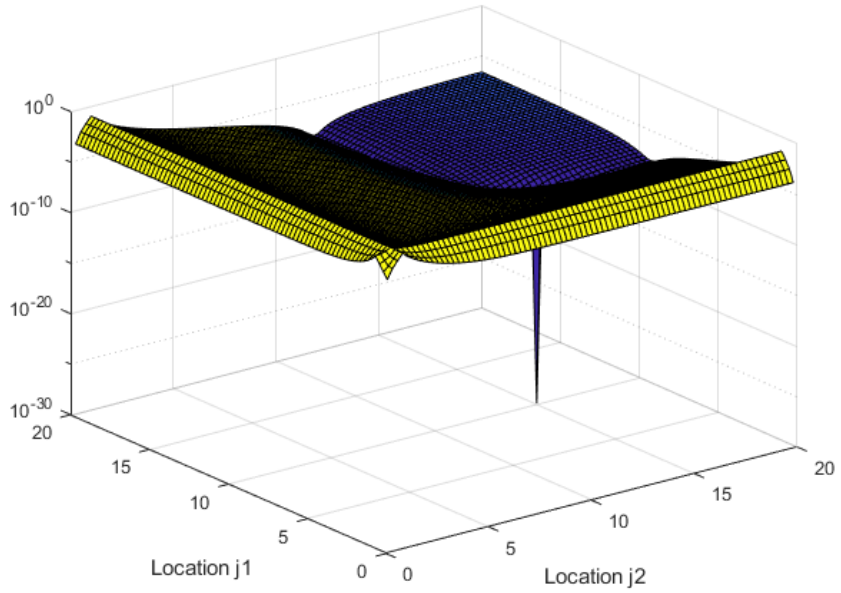

(a) 3D plot of r

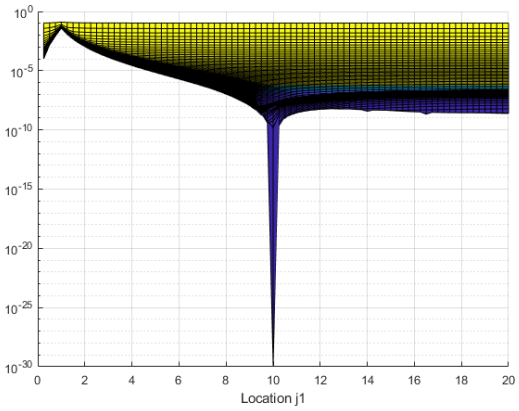

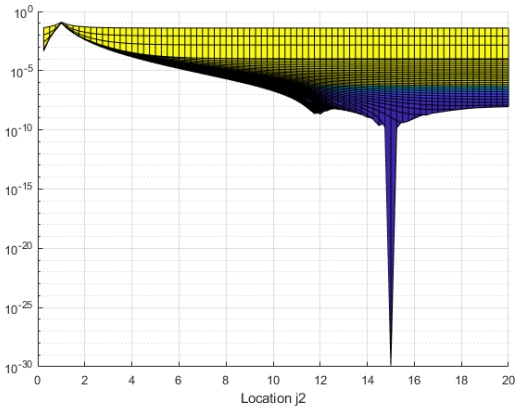

(b) 2D projection of the graph showing the j_1-axis (c) 2D projection of the graph showing the j_2-axis.

Figure 17: Different views of the plot of the L^2 residual function r.

4.2.3 *Two defects with unknown locations and masses.* Now we consider the case when the system has exactly two defects of unknown locations and masses. In (4.23) we derived a formula for $\tilde{x}_1$, but this time j_1, j_2, m_1 and m_2 are all unknown. This makes the residual function

$$r(j_1, m_1, j_2, m_2) = \int_0^{+\infty} |\tilde{x}_1(s, j_1, m_1, j_2, m_2) - \tilde{x}_1^*(s)|^2 \, ds.$$

a function of four variables and hence a graphical inspection of the minimum is not possible. For cases like these, numerical optimization schemes can be employed.

We perform this procedure for four systems of different lengths. The minimization of the residual function r was carried out using Matlab's built-in Genetic Algorithm. The results are shown in Table 1. In all of the systems considered, j_1 was computed accurately up to machine precision. The corresponding masses m_1, were also calculated accurately with relative errors ranging between 0.8% and 3.3%. However the minimization algorithm doesn't perform that well in estimating the parameters of the second defect. Thus, a separate study on designing minimization algorithms better suited to the problem at hand is highly recommended.

Table 1: Results obtained by using Matlab's Genetic Algorithm in minimizing r with respect to j_1, m_1, j_2 and m_2.

	System 1	System 2	System 3	System 4
System Parameters				
n	5	10	20	20
j_1	2	3	8	8
j_2	4	7	15	15
m_1	3	3	5	5
m_2	0.5	2	2	15
Estimates from Mathlab's Genetic Algorithm				
j_1	2	3	8	8
j_2	4	4	17	16
m_1	2.9760	2.9009	5.0113	5.0646
m_2	0.6579	1.3364	3.2586	14.2290

5 Conclusion

In summary, this paper tackled two problems involving Hookean spring-mass systems. In the first half, we introduced a method to compute an active vibration suppression control for a spring-mass system of arbitrary length. We used an alternative approach in solving (2.1) that overcomes the numerical issues raised in [11] that occurs whenever n is large. This was done by solving the problem in the corresponding Laplace domain. In such case, our approach only required a robust numerical integration of the inverse Laplace transform. However, in some applications, a more practical approach that gives a fast and reasonable solution is preferred over a very accurate but computationally expensive method. Hence, modifying the formulas derived here by using some known approximations may be worth looking into.

The second half of the paper deals with identifying the location and size of defects in a system using Laplace domain measurements $\tilde{x}_1(s)$. In the case of exactly one defect of unknown location, the procedure only requires direct calculations involving $\tilde{x}_1(s)$. The formulas were simplified

by using asymptotic estimates with respect to the variable s. When there are more than one unknown defect parameter, we perform the minimization of the L^2 residual function defined in (4.18). Designing a robust algorithm transforming discrete vibration measurements $x_1(t)$ to the corresponding Laplacian data $\tilde{x}_1(s)$ will be a nice follow-up research as it can provide a direct link between the physical experiment setting and the method we developed. Also, a study on finding a better minimization algorithm for the residual function is highly recommended.

Extensions of the work presented here to non-Hookean systems, non-homogeneous materials and springs with varying damping coefficients are very important and will be considered in forthcoming reports.

References

[1] P. Abeyrathna, W.A.S.P. Abeysiriwardhana, S. Amarasinghe, W. Ariyasinghe, and A. Abeykoon, *Simulation on active vibration suppression using virtual spring-damper combination*, IEEE (2013), 1–6.

[2] A. Chavan and Phvithran S., *Simulation and analysis of passive and active suspension system using quarter car model for non uniform road profile*, Int. J. of Eng. Res. and App. **2** (2012), no. 5, 900–906.

[3] W. Clark, *Vibration control with state-switched piezoelectric materials*, Journal of Intelligent Material Systems and Structures **11** (2000), no. 4, 263–271.

[4] L. Corr and W. Clark, *A novel semi-active multi-modal vibration control law for a piezoceramic actuator*, Journal of vibration and acoustics **125** (2003), no. 2, 214–222.

[5] G. Y. Hu and R. F. O'Connell, *Analytical inversion of symmetric tridiagonal matrices*, J.Phys. A:Math.Gen. **29** (1996), 1511–1513.

[6] P. Huang, L. Gu, X. Li, S. Zhang, J. Xu, C. Lin, and Q. Fang, *Real-time simulation for global deformation of soft tissue using deformable centerline and medial representation*, ISBMS (2013), 67–74.

[7] O. Jarrousse, *Modified mass-spring system for physically based deformation modeling*, KIT Scientific Publishing (2012), ISBN10 3866447426.

[8] J. D. Joannopoulos, S. G. Johnson, J. N. Winn, and R. D. Meade, *Photonic crystals, molding the flow of light*, 2^{rd} ed., Princeton Univ. Press, 2008.

[9] T. Liu, A. Bargtail, J. O'Brien, and L. Cavan, *Fast simulation of mass-spring systems*, ACM transactions on graphics **32** (2013), no. 6, 209:1–209:7.

[10] M. Makwana and R.V. Craster, *Localised point defect states in asymptotic models of discrete lattices*, Q. JI Mech. Appl. Math **66** (2013), no. 3, 289–316.

[11] D. Morgan and S. Qiao, *Accuracy and stability in mass-spring systems for sound synthesis*, Proceedings of C3S2E-08 (2008), 1–12.

[12] J. Mosegaard, P. Herborg, and T. S. Sorensen, *A gpu accelerated spring mass system for surgical simulation*, ISBMS **111** (2005), 342–348.

[13] A. Nealan, M. Muler, R. Keiser, E. Boxerman, and M. Carlson, *Physically based deformable models in computer graphics*, Comput. Graph. Forum **25** (2005), no. 4, 809–836.

[14] L. Nedel and D. Thalmann, *Real time muscle deformations using mass-spring systems*, Proceedings of the Computer Graphics International (1998), 157–177.

[15] André Preumont, *Vibration control of active structures, an introduction*, 3^{rd} ed., Solid mechanics and its applications, Springer, 2011.

[16] M. Rababah and A. Bhuyan, *Passive suspension modeling and analysis of a full car model*, Int J. of Adv. Sc. and Eng. Tech. **3** (2013), no. 2, 250–261.

[17] M. El Saif and M. A. Foda, *Vibration suppression of a beam stucture of intermediate masses and springs*, Journal of Sound and Vibration **256** (2001), no. 4, 629–645.

[18] Z. Sarosi, W. Knapp, A. Kunz, and K. Wegener, *Detection of surface defcts on sheet metal parts by using one-shot deflectometry in the infrared range*, FLIR Techical Series (2010).

[19] B. Wie and D. Bernstein, *Robust control design for a benchmark problem*, Journal of guidance, control, and dynamics **15** (1992), no. 5, 1057–1059.

[20] S. Yao, X. Zhou, and G. Hu, *Experimental study on negative mass effective mass in a 1d mass-spring system*, New J. Phys. **10** (2008), no. 4, 1–4.

[21] S. Zhang, L. Gu, P. Huang, and J. Xu, *Real-time simulation of deformable soft tissue based on mass-spring and medial representation*, Computer Vision for Biomedical Image Applications, a workshop of ICCV2005 **LNCS 3875** (2005), 419–426.

[22] F. Zolla, G. Renversez, A. Nicolet, B. Kuhlmey, S. Guenneau, and D. Felbacq, *Foundations of photonic crystal fibres*, Imperial College Press, 2005.